01

Investigation of thermophysical processes of obtaining various aluminum matrix composites

© V.V. Myl'nikov,[1] A.I. Pronin,[2] M.V. Myl'nikova,[1] E.A. Romanova,[1] D.I. Shetulov[1]

[1] Nizhny Novgorod State University of Architecture and Civil Engineering, Nizhny Novgorod, Russia
[2] Komsomolsk-na-Amure State University, Komsomolsk-na-Amure, Russia
e-mail: mrmylnikov@mail.ru

Received September 7, 2022
Revised October 12, 2022
Accepted October 14, 2022

The possibilities of obtaining aluminum matrix composite materials of the composition $Al-Al_2O_3$ are considered by the method of liquid-phase oxidation of aluminum by purging the melt with oxygen. The obtained materials are a two-phase system with different concentrations of the solid phase. An algorithm for calculating the kinetics of aluminum oxidation in obtaining the oxide phase of an aluminum matrix composite is proposed. It is established that the beginning and completeness of the reaction on the surface of the gas bubble determines the synthesis of the oxide phase and is determined by the functions $T(t)$, $h(t)$ in the region of dynamic time delay, which, in turn, the queue is revealed as a function of the temperature in the contact zone of the gas bubble with the melt, taking into account the duration of the heating of the bubble along the cross section and the radius of the bubble itself. The microstructures of the obtained materials with different structural-phase state with variations in the time of purging and oxygen supply to the aluminum melt are presented.

Keywords: aluminum matrix composite material, high temperature oxidation, gas bubble.

Introduction

One of groups of artificially created materials are aluminum matrix composites (AMC) [1]. They are composed of a metal phase based on pure metals or an alloy on their basis and a strengthening phase in the form of oxides, nitrites, etc. At the same time the resulted material has properties, which are considerably different from properties of each individual component included in the AMC, and at the same time partially has properties of metal (for example, plasticity) and ceramics (for example, high hardness and thermal resistance). Many AMCs demonstrate such physical and mechanical and operating characteristics, that are unachievable in traditional materials, even with the use of state-of-the-art hardening technologies [2–6].

The production of AMCs was initially related to the method of powder metallurgy [7]. Modern technologies of aluminum matrix composites production mainly use the melt saturation with the use of powder materials [8,9]. In addition, special attention is currently paid to production of cast aluminum matrix composites by injecting finely dispersed high-melting additions directly in the process of casting (when pouring), which significantly increases the number of crystallization centers when the melt is cooled.

The main problem of AMC production is ensuring physical and chemical compatibility between the matrix and the strengthening phase. Their wide application is constrained by the risk of development of chemical interaction between the matrix and discrete fillers, emergence of interphase joints that embrittle the matrix, and weakening of the connection at the interface between the matrix and the strengthening phase. Since dispersion-hardened composite alloys are heterophase systems with developed network of interphase boundaries, their manufacture is accompanied by actively running processes such as chemical reactions and interdiffusion between the matrix melt and the filler. Production of high-quality AMCs requires this interaction to be restricted, to exclude the strengthening phase degradation resulting in reduction of mechanical and operating properties of cast parts [10,11].

Along with interphase boundaries, a significant role in ensuring strength characteristics is played by dimensions of reinforcing fillers, their geometry, and uniformity of their distribution within the material volume. It should be noted that the complexity of technologies of fillers linkage to matrices, as well as the difficulties related to machining of finished products made of AMCs are additional constraining factors that limit their adoption in production processes.

The presence of these sizeable disadvantages gave a stimulus to the development of new methods to produce AMCs, one of which is the „method of internal melt oxidation“. This method of AMC production reduces the cost of material due to the refusal of powders, and an opportunity arises for a wide flexibility of structural-phase composition of the produced material. The method is based on physical and chemical processes of metal oxidation at high temperatures of melt by oxygen-blowing of liquid metal [12]. The chemical interaction results in synthesis of solid phases: if the metal is oxygen-blown, we get oxides, if it is nitrogen-blown, we get nitrides.

The goal of this work is to study the thermophysical process of ceramic phase synthesis in the aluminum melt when the method of internal oxidation is realized, with identification of main parameters of this process affecting

the structural-phase composition of the produced material and production of aluminum matrix materials with different structural configuration taking into account these parameters.

1. Investigation technique

We took A6 grade aluminum as the raw material to produce the AMC. Chemical composition of the A6 grade according to GOST 11069-2001 is as follows: (Al) 99.6%; (Fe) 0.25%; (Si) 0.2%; (Ti) 0.03%; (Cu) 0.01%; (Zn) 0.06%.

An original stand was developed and designed to implement the under-development method of internal oxidation, which was composed of a high-temperature induction furnace (Fig. 1. item I), a system to store and supply oxygen. Also, the experimental stand included a high-precision gas panel with a needle valve mounted in its output to precisely control the gas supply. The valve was connected to a pressure gauge to monitor the pressure downstream of the needle, which was turning to a conventional ball valve and a variable area flowmeter. Aluminum ingots were charged into the furnace (Fig. 1. item I, melting pot *4*) and melted. Then a silicon carbide tube was introduced into the aluminum melt (Fig. 1. item I, tube *3*) with a system to adjust the tube position vertically *1* and angularly *2*. The tube was leak-tight connected to a steel tube that, in turn, was attached to the variable area flowmeter. This system was used to supply oxygen into the aluminum melt. To protect the aluminum against undesirable oxidation, an atmosphere of inert gas was formed by supplying gas via the tube *5* shown in Fig. 1. As a result of high-temperature chemical reaction

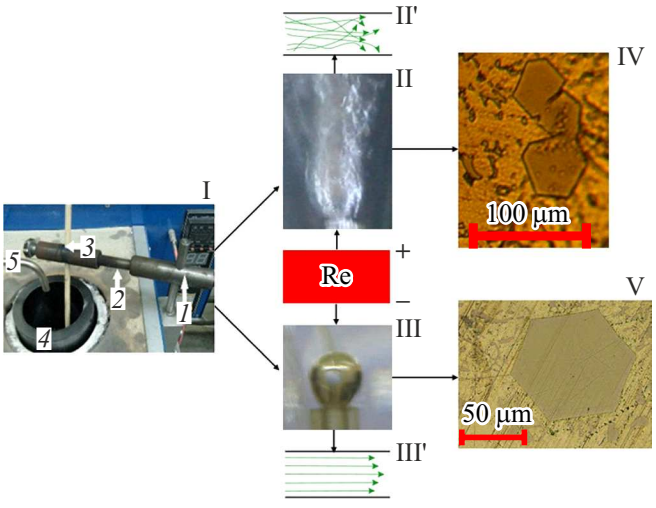

Figure 1. Scheme to produce the strengthening phase: I — working part of the furnace with dismantled thermal insulation; II — jet of the supplied oxidant gas with a typical turbulent motion mode II′; III — single bubble of the oxidant gas with a typical laminar motion mode III′; IV — microstructure obtained as a result of the process II; V — microstructure obtained as a result of process III.

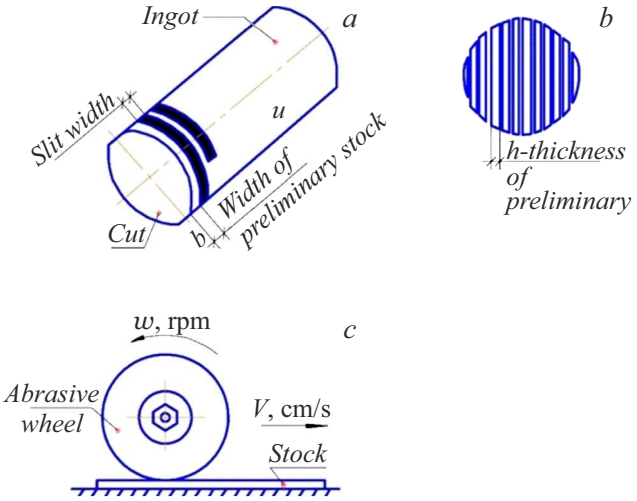

Figure 2. Scheme of samples production for microscopic studying.

$4Al + 3O_2 \rightarrow 2Al_2O_3$ the ceramic phase was synthesized directly in the melt in one stage of the implemented process. To remove casting defects and degassing, the produced material was argon-blown immediately before its pouring into small steel chill molds.

The size of obtained particles of aluminum oxide was varied by replaceable tips in the form of nozzle with different output diameters to produce different sizes of the gas bubbles supplied into the melt, which resulted in a wide range of sizes of the strengthening phase — from nanometer to millimeter order.

The resulted ingots were used to manufacture samples (Fig. 2) for microscopic studying. The resulted ingots were machine-cut in transverse direction to produce workpieces (Fig. 2, *a*), from which samples were cut-off (Fig. 2, *b*) and ground (Fig. 2, *c*).

Then the samples were prepared in accordance with the standard procedure for microstructure examination. For this purpose microsections were processed on a rotating horizontal disc of a SShPM-1 machine with adjustment of the rotating speed. In this case the sample was installed in a special fixture for convenience.

After the grinding, the samples were polished mechanically. The disc for mechanical polishing was wrapped with cloth or felt and moisturized with chrome oxide suspension. The surface of polished samples was washed, degreased, and dried.

For the microstructure studying we used a CRAFTEST CL-720e optical direct microscope, a Keyence VHX-1000 digital microscope for material examinations, and a JEOL JSM-IT300LV and a Hitachi S-3400N scanning electron microscopes.

In some cases, to detect and clarify the configuration of structural-phase composition, the samples were destructed either by rupture or by bending, and the resulted fractures were investigated in the zones of separation and break

Algorithm to calculate kinetics of aluminum oxidation when producing ceramic phase of the metal-ceramic composite

Operation number	Operation content					
I	Initial calculation of the $Al-Al_2O_3$ system					
II	Efficiency and control over production of the ceramic phase Al_2O_3					
III	Calculation of the zone of warm-up rate of oxidation	Estimate of the zone of burning	Intensity of heat release	Calculation of the reaction start time	Estimate of the required reaction time	Hydrodynamics of the metal (solid/liquid/vapor)-oxidant (gas)-ceramics (vapor/liquid/solid) system

to exclude the deformation contribution during material destruction.

2. Results and discussion thereof

It is known that configuration, size, and mutual arrangement of phases in the material structure have a dramatic effect on mechanical properties and operating characteristics. To obtain the set size of aluminum oxide particle, an oxygen bubble must be formed in the melt, which collapses in the process of oxidation resulting in formation of a ceramic particle shown in Fig. 1, item V. This form of oxide as a regular hexagon of almost ideal shape is related with the tetrahedral arrangement of spheres in the hexagonal close pack in conditions of low temperatures and stable laminar motion (Fig. 1, item III′). In the case of gas jet supply into the melt (Fig. 1, item II) a temperature growth is observed, and particles start to melt together forming a structure shown in Fig. 1, item IV, which can be avoided by providing circulation of the metal. Changes in temperature, size, and mass of gas bubbles, as well as polymorphism of aluminum and a large number of modifications of the crystal atomic lattice of corundum should result in a diversity of produced AMC structures, and, as a consequence, different physical and mechanical properties, which is of great interest as well.

Preliminary theoretical studying and initial calculations have shown that to determine efficiency of the aluminum-oxygen system interaction taking into account features of the burning process, oxidation, and control of obtaining the strengthening inclusions of Al_2O_3, it is necessary to identify main calculation criteria and fundamental phenomena affecting them. As a result of the analysis performed, we have suggested an algorithm of such calculation shown in the table in the form of scheme of successive mathematical operations.

In addition, it is necessary to bear in mind the known properties of aluminum:

— oxidability in the process of melting with formation of harmful films that impair the diffusion of oxygen to the metal;

— polymorphism at elevated temperatures accompanied by the transition from γ-modification to α-Al_2O_3.

To describe oxidation of aluminum bubbles on their surface in the melt at a temperature of T_{liq}, we have use the equation of thermophysics that defines the dependence of energy exchange between the bubble and the melt:

$$\frac{dQ}{dt} = \frac{dH}{dt} - \frac{1}{p}\frac{dp}{dt}, \tag{1}$$

where the source of heat and changes in bubble entalphy are defined by the following formulae:

$$\frac{dQ}{dt} = \alpha S(T_{liq} - T), \tag{2}$$

$$\frac{dH}{dt} = \sum H_1 \frac{dy_i}{dt} + mc_p \frac{dT}{dt}. \tag{3}$$

Hence we get

$$\sum H_1 \frac{dy_i}{dt} + mc_p \frac{dT}{dt} = \alpha S(T_{liq} - T), \tag{4}$$

where the change in mass percentage of components is represented as follows

$$\frac{dy_i}{dt} = \frac{\omega_i M_i}{p}$$

taking into account that

$$\omega_i = \left(\frac{dN_i}{dt}\right)_{p,T}.$$

It was shown in the analysis of Fig. 1, that a change in modes III′ (laminar) and II′ (turbulent) results in significant structural rearrangements with observed changes in heat emission coefficients (HEC) that depend in the flow velocity and defined by Reynolds criteria:

— with increase (Fig. 1) in $\mathrm{Re} \geq 0.92 \cdot 10^4$ mode II′ is observed with HEC:

$$\alpha_{liq} = \lambda_{liq}\left[2.5 + 3.6\left(\frac{\omega l}{a_{liq}}\right)^{2/3} \Big/ l\right]; \tag{5}$$

— with decrease (Fig. 1) in $\mathrm{Re} \leq 0.92 \cdot 10^3$ mode III′ is observed with HEC:

$$\alpha_{liq} = 0.75\lambda_{liq}\left[\left(1 + \frac{\omega l}{a_{liq}}\right)^{1/3}\frac{\omega l}{a_{liq}}\right]^{1/2} \Big/ l, \tag{6}$$

where λ_{liq} — kinematic viscosity coefficient, ω — flow velocity, l — characteristic dimension, a_{liq} — thermal conductivity of the melt.

In the aluminum melt at flow velocities close to zero, thermal conductivity of the melt is as high as $a_{liq} \sim 100\,\mathrm{kW/(m^2 \cdot K)}$, while with an increase in aluminum melt velocity of up to $\omega = 0.1\,\mathrm{m/s}$ the value of a_{liq} grows and reaches $420\,\mathrm{kW/(m^2 \cdot K)}$.

To solve the problem of warming up, we make use of the heat balance equation:

$$qF_{\text{eff}}\,d\tau = Mc\,dT, \tag{7}$$

where q — density of the heat flux onto the surface, $[\mathrm{W/m^2}]$; F_{eff} — effective heat-absorbing surface, $[\mathrm{m^2}]$; τ — time, [s]; M — mass, [kg]; c — specific heat capacity, [kJ/(kg·K)]; T — temperature, [K].

By expressing q through the effective heat-exchange coefficient from the melt to the popup bubble α_{liq}, integrating equation (7), and solving for $T_{\text{b.f}}$, we get

$$T_{\text{b.f}} = (T_{liq} - T_{\text{b.b}})[1 - \exp(-\alpha_{liq}F_{\text{eff}}\tau/Mc)] + T_{\text{b.b}}, \tag{8}$$

where T_{liq}, $T_{\text{b.b}}$, and $T_{\text{b.f}}$ are temperature of the melt, start and end temperatures of the bubble.

By solving this equation for time, we get

$$\tau = (Mc/\alpha_{liq}F_{\text{eff}})\ln\left[(T_{liq} - T_{\text{b.b}})/(T_{liq} - T_{\text{b.f}})\right]. \tag{9}$$

Thus, the equation of bubble warming up will take the following form:

$$\rho c_p \frac{\partial T}{\partial t} = \frac{\partial}{\partial r}\left(\lambda\frac{\partial T}{\partial r}\right) + \frac{2}{r}\frac{\partial T}{\partial r}\ \big(0 < r < R(t)\big), \tag{10}$$

where ρ — gas density, $[\mathrm{kg/m^3}]$; c_p — specific heat capacity of the gas at $P = \text{const}$, $[\mathrm{J/(kg \cdot K)}]$; T — temperature, [K]; t — time, [s]; $R(t)$ — bubble radius; λ — thermal conductivity coefficient, $[\mathrm{W/(m \cdot K)}]$.

It is known that the oxide film covering the aluminum surface at normal environmental conditions significantly impairs the diffusion of oxygen to the metal, therefore thickness of this film has a strong effect on the process of high-temperature oxidation.

Let us make use of kinetics equations to describe the process with accelerated growth of oxide film. The most frequently used are equations of exponential law:

$$\frac{dh}{dt} = KC_{ox}^{m}\exp\left(-\frac{E}{RT}\right)\exp\left(-\frac{h}{h_0}\right) \tag{11}$$

Figure 3. AMC ingots of the $\mathrm{Al-Al_2O_3}$ system with percentage of ceramic phase growing from left to right.

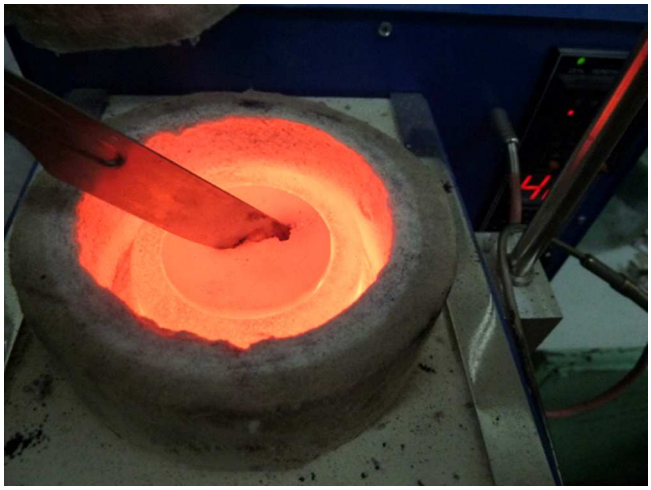

Figure 4. AMC sample of the $\mathrm{Al-Al_2O_3}$ system heated up to 1040°C.

or

$$\frac{dh}{dt} = \frac{KC_{ox}^{m}}{h^n}\exp\left(-\frac{E}{RT}\right), \tag{12}$$

where h — thickness of the oxide film, h_0 — thickness of the oxide film at the initial moment of time, E — activation energy, R — absolute gas constant, K — preexponential factor in the oxidation law, C_{ox} — oxidant concentration at the bubble surface, m — reaction order with respect to oxidant.

The heat balance equation will be expressed as follows:

$$m_p c_p \frac{dT}{dt} = -Sk(T - \tilde{T}) + Sqp_{\mathrm{Al_2O_3}}\frac{dh}{dt} \tag{13}$$

with initial conditions of $t = 0$, $T = T_0$, $h = h_0$, where subscript „0“ denotes initial conditions; m_p, S, c_p — Mass, surface are, and heat capacity, respectively; $p_{\mathrm{Al_2O_3}}$ — density of the oxide; q — reaction heat; $k = \lambda Nu/d$ — heat-exchange coefficient: λ — thermal conductivity coefficient of the gas, Nu — Nusselt number.

As can be seen from the presented formulae, the beginning and extent of reaction on the gas bubble surface (which finally defines the synthesis of the strengthening phase) is defined by $T(t), h(t)$ functions in the region of dynamic time delay, which, in turn, is manifested as a function of temperature in the zone of gas bubble contact with the melt taking into account the duration of bubble warming up over the cross-section and radius of the bubble itself. It is necessary to note that the preexponential factor K and the activation energy of oxidation rate E, although considered as physical-chemical constants, are considerably different in the literature [13–15], which is also related to difficulties of determining the functional link between temperature change and bubble radius.

Thus, the fundamental parameters of $\mathrm{Al_2O_3}$ ceramics production in the Al melt in the process of AMC production will be radius (r) and mass (m) of bubble, which are inseparably related by a functional link to pressure (P)

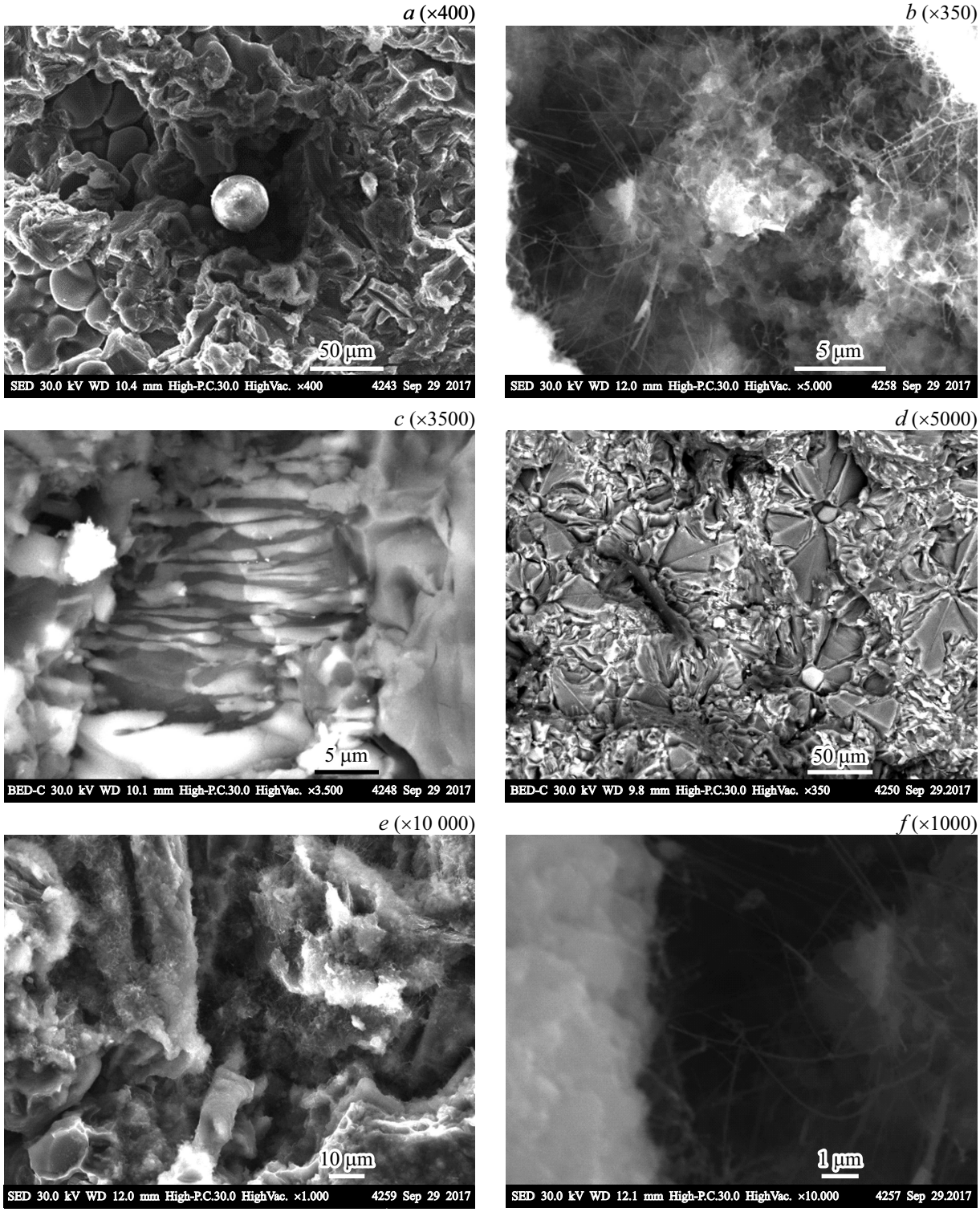

Figure 5. Microstructures of materials with different structural states produced with different variations of the proposed technology.

inside the bubble and volume (V) in the conditions of operating temperature (T):

$$m = f(P, V, T), \quad \text{where} \quad V = 3/4\pi r. \tag{14}$$

For the case of regular hexagon particles, as shown in Fig. 1, with a height of (b), the volume can be determined as follows:

$$V = (3a^2\sqrt{3})b, \tag{15}$$

where a is hexagon side.

This theoretical studying is confirmed by results of searching experiments of production of AMCs with different

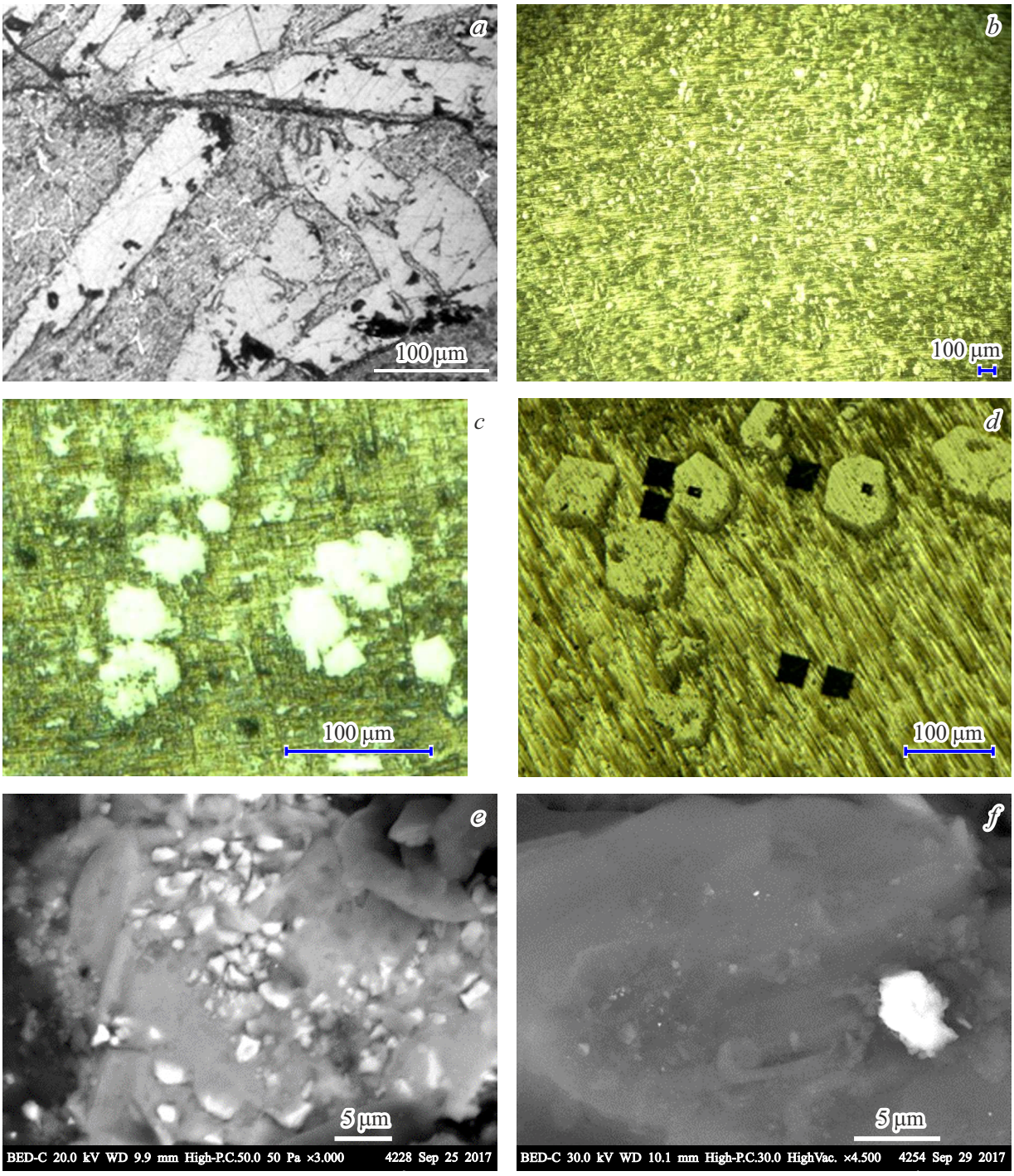

Figure 6. AMC structures with different sizes of ceramic phase: *a* — example of solid fraction with a size of plate-shaped inclusions greater than 1 mm; *b* — microstructure of the produced material, example of distance measurement: average size of predominantly spherical particles is 10 μm; *c* — average size of flake-like particles is 40 μm; *d* — particles of predominantly hexagonal shape and insignificant number of tetrahedral shape. Average size of particles is 40 μm. PMT-3 microhardness test indentations can be seen; *e* — average size of particles is 1 μm ($\times$3000); *f* — nanodimensions ($\times$4500). A conglomeration of disperse phase can be seen.

structural-phase and percent contents of ceramic components in the alloys.

Fig. 3 shows AMC ingots based on aluminum with different content of the strengthening phase, produced at different times of melt blowing with gas. An increase in blowing time results in growth of the Al_2O_3 percentage in the produced material.

It should be noted, that an increase in Al_2O_3-phase in the AMC composition over 50% (this is a rough value, because size of the phase needs to be taken into account

as well) results in a situation when casting properties of the material are nearly depleted and it becomes difficult to produce samples or parts by casting technological methods. Fig. 4 shows an alloy at a temperature of 1040°C, which has been cut by knife for illustration purposes.

Changes in the supply rate and quantity of gas introduced into the melt result in significant changes in temperature in the zone of oxidation, which, in turn, result in polymorphous transitions of different kinds accompanied by changes in the atom arrangement in the structure and, finally, it manifests in different kinds of geometrical configuration of the solid phase. In the course of experiments, quantity of the strengthening phase in the AMC composition was regulated by means of the blowing time, which was from 10 min to 2 h. To improve throughput and reduce duration of the process, we applied nozzle tips with several holes.

Fig. 5 shows microstructures of produced material at different variations of the process in order to confirm the possibilities of structure configuration changes in a wide range of sizes and shapes: spherical (Fig. 5, *a*) and spade-like (Fig. 5, *d*) shape of microsize scale, columnar (Fig. 5, *c*) and filament shape of nanosize scale (Fig. 5, *b*, *f*), with a structure of „wadding" (Fig. 5, *e*).

Different kinds of microstructures of produced materials with various sizes of strengthening phase are shown in Fig. 6.

Conclusion

In this work we have produced aluminum matrix composites by the method of high-temperature oxidation with different percentage and shapes of the strengthening phase. It is shown experimentally that size of the solid phase synthesized in the aluminum melt is defined by the radius of bubble of the introduced oxygen. At the same time rate and supply of the gas into the melt have the key effect on temperature of the aluminum–oxygen system, accompanied by polymorphous transformations, which finally is manifested in production of the strengthening phases in different geometrical configurations of microstructure of the produced material.

The analysis of features of the oxidation and physics of the burning of aluminum at a high-temperature reaction with oxygen and estimate of the ceramic phase production control have shown that the beginning and extent of reaction on the gas bubble surface finally defines the synthesis of the strengthening phase and is defined by functions of temperature and oxide film thickness in the region of dynamic time delay which, in turn, is manifested as a function of temperature in the zone of gas bubble contact with the melt taking into account the duration of bubble warming up over the cross-section and radius of the bubble itself.

Funding

The study was funded by a grant from the Russian Science Foundation № 22-13-20009, https://rscf.ru/project/22-13-20009/.

Conflict of interest

The authors declare that they have no conflict of interest.

References

[1] E.N. Kablov, *Aviatsionnye materialy i tekhnologii* (VIAM, M., 2012), p. 7–17 (in Russian)
[2] V.B. Deev, E.S. Prusov, E.Kh. Ree, Izv.vuz. Tsvetnaya Metallurgiya, **28** (2), 43 (2022) (in Russian). https://doi.org/10.17073/0022-3438-2021-2-43-59
[3] Z. Yu, G. Wu, L. Jiang, D. Sun. Mater. Lett., **59** (18), 2281 (2005).
[4] C.-H. Jeon, Y.-H. Jeong, J.-J. Seo, H.N. Tien, S.-T. Hong, Y.-J. Yum, S.-H. Hur, K.-J. Lee. Intern. J. Precision Engineer. Manufacturing, **15** (6), 1235 (2014).
[5] R. Purohit, M.M.U. Qureshi, B. Kumar. Mater. Today: Proceedings, **4** (4), 5357 (2017).
[6] S. Mavhungu, E. Akinlabi, M. Onitiri, F. Varachia. Procedia Manuf., **7**, 178 (2017). DOI: 10.1016/j.promfg.2016.12.045
[7] P.K. Rohatgi, P. Ajay Kumar, N.M. Chelliah, T.P.D. Rajan. JOM, **72** (8), 2912 (2020). DOI:10.1007/s11837-020-04253-x
[8] E.S. Prusov, A.A. Panfilov, V.A. Kechin, I.V. Gavrilin, Liteishchik Rossii, **9**, 16 (2012) (in Russian)
[9] V. Deev, E. Prusov, E. Ri, O. Prihodko, S. Smetanyuk, X. Chen, S. Konovalov. Metals, **11** (9), 1353 (2021). https://doi.org/10.3390/met11091353
[10] T.A. Chernyshova, Yu.A. Kurganova, L.I. Kobeleva, L.K. Bolotova, *Litye dispersno-uprochyonnye alyumomatrichnye komozitsionnye materialy: izgotovlenie, svoistva, primenenie* (UGTU, Ulyanovsk, 2012) (in Russian)
[11] Y.A. Kurganova, A.G. Kolmakov, Chen' Itszin', S.V. Kurganov. Inorganic Materials: Appl. Research. **13** (1), 157 (2022). DOI: 10.1134/S2075113322010245
[12] E.A. Chernyshov, A.D. Romanov, E.A. Romanova, V.V. Myl'nikov, Izv. vuz. Poroshkovaya metallurgiya i funktsional'nye pokrytiya, **4**, 29 (2017) (in Russian)
[13] A.G. Merxhanov, A.S. Mukasyan, *Tverdoplamennoe gorenie* (Torus Press, M., 2007) (in Russian)
[14] A.S. Rogachev, A.S. Mukasyan, *Gerenie dlya sinteza materialov: vvedenie v strukturnuyu makrokinetiku* (Fizmatlit, M., 2012) (in Russian)
[15] Yu.E. Sheludyak, L.Ya. Kashporov, L.A. Malinin, V.N. Tsalkov, *Teplofizicheskie svoistva komponentov goryuchikh sistem* (Inform TEI, M., 1992) (in Russian)